Appl Phys A (2008) 93: 549–558
DOI 10.1007/s00339-008-4667-z

Applied Physics A
Materials Science & Processing

Structure, electrical properties and temperature characteristics of $Bi_{0.5}Na_{0.5}TiO_3$–$Bi_{0.5}K_{0.5}TiO_3$–$Bi_{0.5}Li_{0.5}TiO_3$ lead-free piezoelectric ceramics

Dunmin Lin · Qiaoji Zheng · Chenggang Xu · K.W. Kwok

Received: 28 April 2008 / Accepted: 11 May 2008 / Published online: 3 June 2008

Abstract $(1-x-y)Bi_{0.5}Na_{0.5}TiO_3$–$xBi_{0.5}K_{0.5}TiO_3$–$yBi_{0.5}Li_{0.5}TiO_3$ lead-free piezoelectric ceramics have been prepared by an ordinary sintering technique, and their structure, electrical properties, and temperature characteristics have been studied systematically. The ceramics can be well-sintered at 1050–1150 °C. The increase in K^+ concentration decreases the grain-growth rate and promotes the formation of grains with a cubic shape, while the addition of Li^+ decreases greatly the sintering temperature and assists in the densification of BNT-based ceramics. The results of XRD diffraction show that K^+ and Li^+ diffuse into the $Bi_{0.5}Na_{0.5}TiO_3$ lattices to form a solid solution with a pure perovskite structure. As x increases from 0.05 to 0.50, the ceramics transform gradually from rhombohedral phase to tetragonal phase and consequently a morphotropic phase boundary (MPB) is formed at $0.15 \leq x \leq 0.25$. The concentration y of Li^+ has no obvious influence on the crystal structure of the ceramics. Compared with pure $Bi_{0.5}Na_{0.5}TiO_3$, the partial substitution of K^+ and Li^+ for Na^+ lowers greatly the coercive field E_c and increases the remanent polarization P_r of the ceramics. Because of the MPB, lower E_c and large P_r, the piezoelectricity of the ceramics is improved significantly. For the ceramics with the compositions near the MPB ($x = 0.15$–0.25 and $y = 0.05$–0.10), the piezoelectric properties become optimum: piezoelectric coefficient $d_{33} = 147$–231 pC/N and planar electromechanical coupling factor $k_P = 20.2$–41.0%. In addition, the ceramics exhibit relaxor characteristic, which probably results from the cation disordering in the 12-fold coordination sites. The depolarization temperature T_d shows a strong dependence on the concentration x of K^+ and reaches the lowest values at the MPB. The temperature dependences of the ferroelectric and dielectric properties at high temperatures may imply that the ceramics may contain both the polar and non-polar regions at temperatures above T_d.

PACS 77.65.-j · 77.84.Dy · 77.84.-s

1 Introduction

Lead-based piezoelectric ceramics with perovskite structure, represented by lead zirconate titanate (PZT) and PZT-based multi-component systems, are widely used for actuators, sensors, transducers as well as other electromechanical devices due to their excellent electrical properties near the MPB. However, because of the high toxicity of lead oxide and its high volatility during sintering, the use of lead-based materials has caused serious lead pollution and environmental problems. Therefore, there is an increasing interest in developing lead-free ceramics with good properties.

$Bi_{0.5}Na_{0.5}TiO_3$ (BNT), discovered by Smolenskii et al. in 1960 [1], is considered as one of the good candidates for lead-free piezoelectric ceramics because of a large remanent polarization ($P_r = 38.0\ \mu C/cm^2$) at room temperature [2]. However, pure BNT ceramic has a high coercive field ($E_c = 7.3$ kV/mm) [2], making the poling of the ceramic extremely difficult. Thus, the pure BNT ceramic usually exhibits very poor piezoelectricity ($d_{33} = 58$ pC/N) [3]. To lower the coercive field and improve the

D. Lin (✉) · Q. Zheng · C. Xu
College of Chemistry and Materials Science, Sichuan Normal University, Chengdu 610066, People's Republic of China
e-mail: ddmd222@yahoo.com.cn

K.W. Kwok
Department of Applied Physics and Materials Research Centre, The Hong Kong Polytechnic University, Kowloon, Hong Kong, People's Republic of China

piezoelectric properties, a number of solid solutions of BNT with ABO_3-type ferroelectrics or non-ferroelectrics, such as BNT–$Bi_{0.5}K_{0.5}TiO_3$ [4–7], BNT–$BaTiO_3$ [1, 8], BNT–$Bi_{0.5}K_{0.5}TiO_3$–$KNbO_3$ [9], BNT–$NaNbO_3$ [10], La-doped BNT–$BaTiO_3$ [11], BNT–$BaTiO_3$–$Bi_{0.5}Li_{0.5}TiO_3$ [12], BNT–$Bi_{0.5}K_{0.5}TiO_3$–$BaTiO_3$ [13–18], BNT–(Ba, Sr, Ca)TiO_3 [19] and $(Bi_{0.5}Na_{0.5})_{0.94}Ba_{0.06}Zr_yTi_{1-y}O_3$ [20], have been studied extensively. After the formation of solid solutions, the coercive filed of the ceramics is lowered significantly and the MPB is formed, and thus the improved piezoelectric properties are obtained. Generally, for lead-based materials, it has been known that multi-component ceramics possess better piezoelectric properties than single or binary-component ceramics because of the formation of the MPB, and hence R&D effort has always been put on developing new multi-component piezoelectric ceramics. On the basis of the reported work on BNT-based ceramics [1–20] and the analogy of PZT-based ceramics, a new ternary K- and Li-co-modified BNT-based solid solution, $(1-x-y)Bi_{0.5}Na_{0.5}TiO_3$–$xBi_{0.5}K_{0.5}TiO_3$–$yBi_{0.5}Li_{0.5}TiO_3$, has been developed in our precious study and the piezoelectricity of several compositions has been reported [21]. However, little is known about the microstructure, phase transformation, dielectric properties, and temperature characteristics of the ceramics. In the present work, $(1-x-y)Bi_{0.5}Na_{0.5}TiO_3$–$xBi_{0.5}K_{0.5}TiO_3$–$yBi_{0.5}Li_{0.5}TiO_3$ ceramics were prepared by a conventional ceramic fabrication technique, and their microstructures, phase transformation, electrical properties (dielectric, ferroelectric, and piezoelectric) and temperature characteristics were studied systematically.

2 Experimental

A conventional ceramic fabrication technique was used to prepare $(1-x-y)Bi_{0.5}Na_{0.5}TiO_3$–$xBi_{0.5}K_{0.5}TiO_3$–$yBi_{0.5}Li_{0.5}TiO_3$ lead-free ceramics (BNT–BKT–BLT–x/y) using analytical-grade metal oxides or carbonate powders as raw materials: Bi_2O_3 (99%), Na_2CO_3 (99%), K_2CO_3 (99.8%), Li_2CO_3 (97%), and TiO_2 (99.5%). The powders in the stoichiometric ratio of the compositions were mixed thoroughly in ethanol using zirconia balls for 8 h, then dried and calcined at 850 °C for 2 h. After the calcination, the mixture was ball-milled again and mixed thoroughly with a polyvinyl alcohol (PVA) binder solution, and then pressed into disk samples. The disk samples were finally sintered at 1050–1150 °C for 2 h in air. Silver electrodes were fired on the top and bottom surfaces of the samples for the subsequent poling and measurements. The samples were poled under a dc field of 4–6 kV/mm at 60 °C in a silicon oil bath for 20 min.

The crystalline structure of the sintered samples was examined using X-ray diffraction (XRD) analysis with CuK_α radiation (DX-1000). The microstructures were observed using scanning electron microscopy (JSM-5900LV). The relative permittivity ε_r and loss tangent $\tan\delta$ of the ceramics at 1 kHz, 10 kHz, and 100 kHz were measured as a function of temperature using an impedance analyzer (HP 4192A). A conventional Sawyer–Tower circuit was used to measure the polarization hysteresis (P–E) loop at 50 Hz. The electromechanical coupling factor k_p was determined by the resonance method according to the IEEE Standard 176 using an impedance analyzer (HP 4294A). The piezoelectric coefficient d_{33} was measured using a piezo-d_{33} meter (ZJ-3A, China).

3 Results and discussion

Figure 1 shows the SEM micrographs of the BNT–BKT–BLT–x/y ceramics with x/y = 0.10/0.10, 0.20/0.10, 0.30/0.10, 0.15/0.05, 0.15/0.10, and 0.15/0.15. All the ceramics can be well-sintered at 1050–1150 °C for 2 h, and are dense and pore-free, giving a high relative density (>97%). The substitution of K^+ for Na^+ leads to an obvious change in the grain shape and size. For the BNT–BKT–BLT–0.10/0.10 ceramics, the grains have a diameter in the range of 2.5 μm to 3 μm (Fig. 1a). As the substitution level x of K^+ increases from 0.10 to 0.30, the grains become significantly smaller (1.0 μm to 1.50 μm) and grow into clear and neat rectangular shapes (Figs. 1b–c). The increase in K^+ concentration decreases the grain-growth rate and promotes the formation of grains with a cubic shape. The effect of K^+ on grain growth in the present ceramics is similar to that in the BNT–$Bi_{0.5}K_{0.5}TiO_3$ [6, 7, 22] and BNT–$Bi_{0.5}K_{0.5}TiO_3$–$BaTiO_3$ ceramics [14, 18]. On the other hand, different from the concentration x of K^+, the concentration y of Li^+ in the BNT–BKT–BLT–0.15/y ceramics has relatively weak influence on the grain size and shape. With the concentration y of Li^+ increasing, the grain become slightly smaller and more rectangular, and the ceramics are denser (Figs. 1d–f). It can be noted that the introduction of Li^+ lowers significantly the sintering temperature. Generally, Li-free BNT-based ceramics [2–11, 13–18], such as pure BNT [2], BNT–$Bi_{0.5}K_{0.5}TiO_3$ [4–7], BNT–$BaTiO_3$–$Bi_{0.5}K_{0.5}TiO_3$ [13–18] and BNT–$BaTiO_3$ [1, 8, 11], can be sintered to obtain dense ceramics at 1175–1250 °C. However, after the addition of Li^+, the present ceramics can be well-sintered at 1050–1150 °C. Therefore, it can be concluded that the addition of Li^+ decreases the sintering temperature of BNT-based ceramics by 125–200 °C and thus greatly assists in the densification of BNT-based ceramics, which should be attributed to the formation of liquid phase during sintering due to the low melting point of Li-containing compounds.

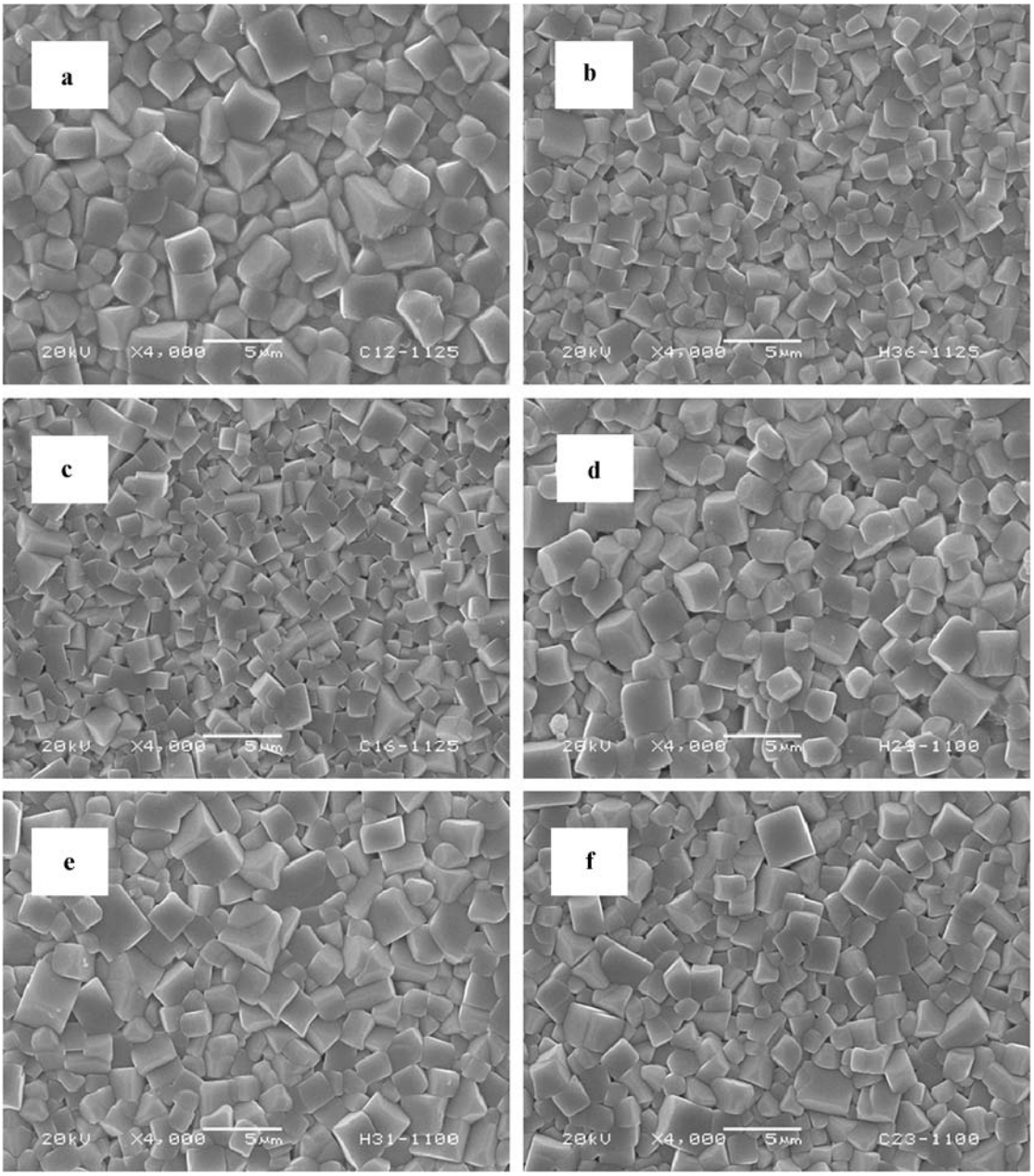

Fig. 1 SEM micrographs of the BNT–BKT–BLT–x/y ceramics: (**a**) $x/y = 0.10/0.10$ sintered at 1125 °C for 2 h; (**b**) $x/y = 0.20/0.10$ sintered at 1125 °C for 2 h; (**c**) $x/y = 0.30/0.10$ sintered at 1125 °C for 2 h; (**d**) $x/y = 0.15/0.05$ sintered at 1100 °C for 2 h; (**e**) $x/y = 0.15/0.10$ sintered at 1100 °C for 2 h; and (**f**) $x/y = 0.15/0.15$ sintered at 1100 °C for 2 h

The XRD patterns of BNT–BKT–BLT–$x/0.10$ and BNT–BKT–BLT–$0.15/y$ ceramics are shown in Figs. 2 and 3, respectively. All the ceramics has a pure perovskite structure and no second phases can be detected, suggesting that K^+ and Li^+ diffuse into the $Bi_{0.5}Na_{0.5}TiO_3$ lattices to form a homologous solid solution (Figs. 2a and 3a). In agreement with the reported work [2, 3, 19], the pure BNT ceramic (i.e., $x = 0$ and $y = 0$) has a rhombohedral symmetry. As shown in Fig. 2b, similar to the pure BNT, only the 202 characteristic peak is observed near 46.5–47.5° for the BNT–BKT–BLT–$x/0.10$ ceramics with $x < 0.15$, suggesting that the ceramics possess a perovskite structure with rhombohedral symmetry. However, it is noted that as x increases from 0.05 to 0.50, the BNT–BKT–BLT–$x/10$ ceramics gradually transforms to a tetragonal symmetry. This is evidenced by the splitting of the (202) diffraction peak to (002) and (200) peaks as observed in the BNT–BKT–BLT–$x/0.10$ ceramics near 46.5–47.5° (Fig. 2b). At $x > 0.25$, the ceramics possess a perovskite structure with tetragonal symmetry. These results are in agreement with the previous work on BNT–

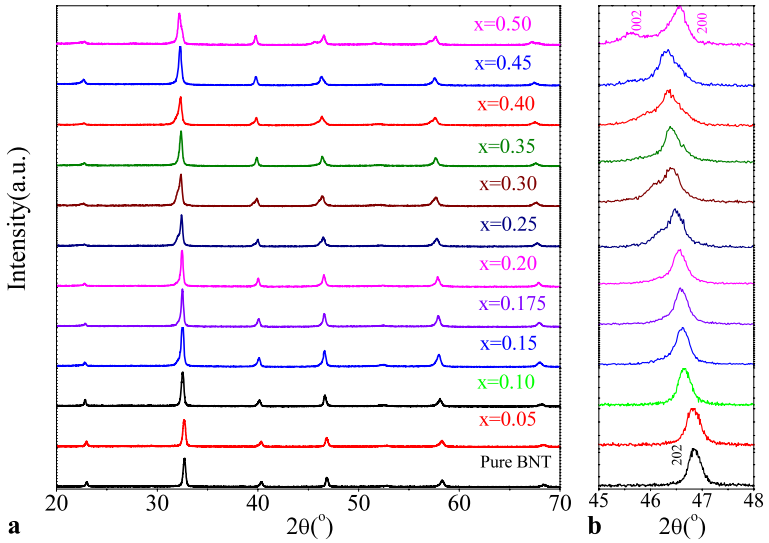

Fig. 2 XRD patterns of the BNT–BKT–BLT–$x/0.10$ ceramics

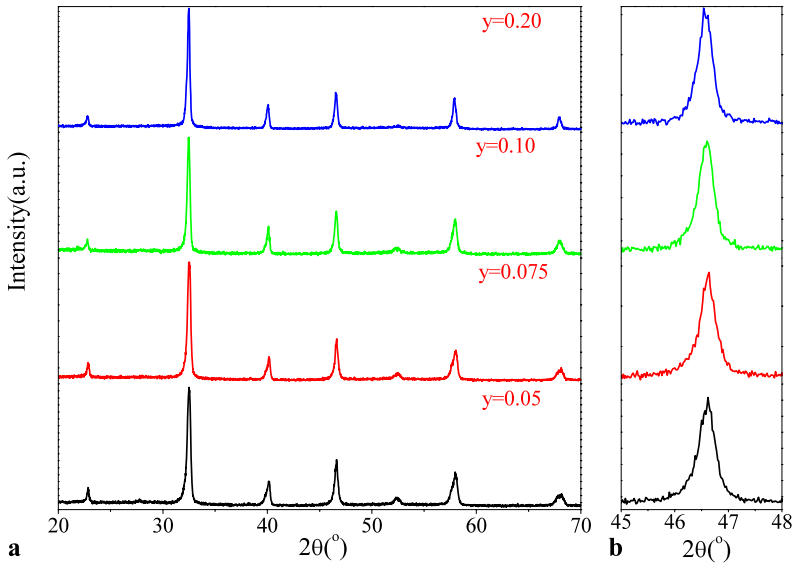

Fig. 3 XRD patterns of the BNT–BKT–BLT–0.15/y ceramics

$Bi_{0.5}K_{0.5}TiO_3$ ceramics [4–7] and suggest that the MPB of rhombohedral and tetragonal phases is formed in the BNT–BKT–BLT–$x/0.10$ ceramics with $0.15 \leq x \leq 0.25$. Different from K^+, it can be seen from Fig. 3 that the concentration y of Li^+ has no significant influence on the crystal structure of the BNT–BKT–BLT–0.15/y ceramics.

As the above mentioned, the pure BNT ceramics has a high coercive field ($E_c = 7.3$ kV/mm), and therefore it is difficult to pole fully. However, in the present work, $Bi_{0.5}K_{0.5}TiO_3$ (BKT) and $Bi_{0.5}Li_{0.5}TiO_3$ (BLT) are introduced into BNT to decrease significantly the coercive field E_c. Figure 4, for example, shows the P–E loops of the BNT–BKT–BLT–$x/0.10$ ceramics with $x = 0.05$, 0.20, and 0.40, while the variations of P_r and E_c with x for the BNT–BKT–BLT–$x/0.10$ ceramics and y for the BNT–BKT–BLT–0.15/y ceramics are shown in Fig. 5. All the ceramics exhibit saturated and typical P–E loops for ferroelectrics under an ac field of 8 kV/mm (Fig. 4). Similar to BNT–$BaTiO_3$ [14], BNT–$Bi_{0.5}K_{0.5}TiO_3$ [4, 14] and BNT–$Bi_{0.5}K_{0.5}TiO_3$–$BaTiO_3$ [14, 15], the ceramics situated at or near the rhombohedral side of the MPB (e.g., BNT–BKT–BLT–0.05/0.10) exhibit larger polarization hysteresis, which gives rise to higher E_c and larger P_r (Fig. 4a), while the compositions situated at or near the tetragonal side of the MPB (e.g., BNT–BKT–BLT–0.40/0.10) show the higher apparent permittivity (Fig. 4c), which can be calculated from the slope gradient of the P–E loop at zero electric field. From Fig. 5a, it can be found that for the BNT–BKT–BLT–$x/0.10$ ceramics, P_r increases slightly with x increasing and then decreases greatly, giving a maximum value of 37.0 μC/cm^2 at $x = 0.20$. The E_c decreases quickly from 6.17 kV/mm to 2.46 kV/mm as x increases from 0.05 to 0.25 and then increases slowly to 3.84 kV/mm with x further increasing to 0.50. Obviously, the BNT–BKT–BLT–$x/0.10$ ceramics with

$0.15 \leq x \leq 0.25$ situated within the MPB possess the largest P_r and lowest E_c. From Fig. 5b, the substitution of 5.0–7.5% Li^+ for Na^+ in the BNT–BKT–BLT–0.15/y ceramics increases the P_r of the ceramics and the maximum value of P_r of 38.8 μC/cm^2 for the BNT–BKT–BLT–0.15/y ceramics reaches at $y = 0.05$–0.075. The E_c increases slightly from 4.10 kV/mm to 4.62 kV/mm as y increases from 0 to 0.125 and then decreases to 3.83 kV/mm with y further increasing to 0.15. Clearly, after the partial substitutions of K^+ and Li^+ for Na^+ in the A-site of BNT, the BNT–BKT–BLT–x/y ceramics exhibit a larger P_r and a lower E_c as compared to a pure BNT ceramic ($P_r = 38$ μC/cm^2 and $E_c = 7.3$ kV/mm).

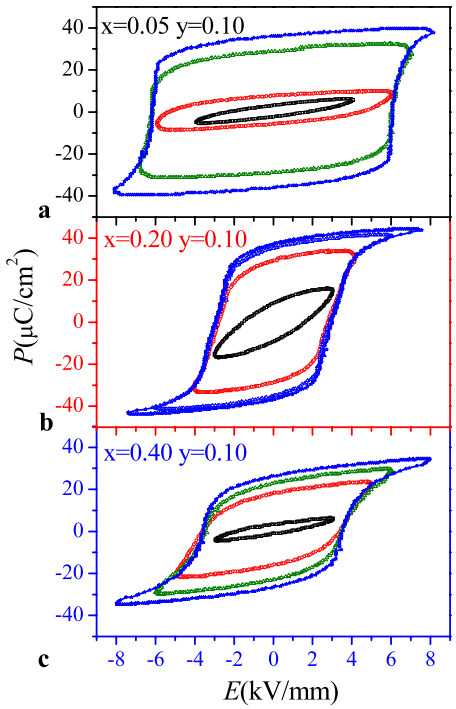

Fig. 4 P–E hysteresis loops of the BNT–BKT–BLTvx/0.10 ceramics with $x = 0.05$, 0.20, and 0.40

The variations of d_{33}, k_p, ε_r, and $\tan\delta$ for the BNT–BKT–BLT–x/y ($y = 0.05$ and 0.10) ceramics with x are shown in Fig. 6, while Fig. 7 shows the variations of piezoelectric and dielectric properties for the BNT–BKT–BLT–x/y ($x = 0.15$ and 0.20) ceramics with y. For the BNT–BKT–BLT–x/y ($y = 0.05$ and 0.10) ceramics, the observed d_{33} and k_p increase sharply with increasing x and then decrease, reaching a maximum value at $x = 0.20$. From Fig. 6a and b, the BNT–BKT–BLT–x/0.10 ceramics with $x = 0.15$–0.20 possess the optimum piezoelectric properties: $d_{33} = 147$–231 pC/N and $k_p = 20.2$–41.0%. Similar to the dependences of d_{33} and k_p on x, the relative permittivity ε_r and loss tangent $\tan\delta$ reach the maximum value at $x = 0.20$–0.25. From Fig. 7a–b, after the addition of 5.0–10% of BLT, the piezoelectricity of the BNT–BKT–BLT–x/y ($x = 0.15$ and 0.20) ceramics is enhanced. Different from d_{33} and k_p, the observed ε_r and $\tan\delta$ increase with y increasing. On the basis of these results (Figs. 6 and 7), it is clearly seen that the BNT–BKT–BLT–x/y ceramics exhibit much better piezoelectric properties than the pure BNT ceramic ($d_{33} = 58$ pC/N) [3]. The significant improvement in electrical properties of the BNT–BKT–BLT–x/y ceramics should be attributed to the formation of the MPB (Fig. 2), lower E_c and larger P_r (Figs. 4 and 5). It is well know that the MPB plays a very important role in the improvement of piezoelectric properties of perovskite piezoelectric ceramics because the number of possible spontaneous polarization directions increases at the MPB. The lower E_c makes the ceramics easily poled, while the large P_r favors the piezoelectricity. On the other hand, compared with Li-free BNT-based ceramics (e.g., BNT–BKT [5], BNT–BKT–BT [16], BNT–BT [2] ($d_{33} = 126$ pC/N, 135 pC/N, and 125 pC/N, respectively), Li-modified BNT–BKT ceramics (i.e., BNT–BT–BLT–x/y) exhibit much stronger piezoelectricity, which should be attributed to the significant improvement in the sintering performance and the increase in P_r after the addition of Li^+.

Figure 8 shows the temperature dependences of ε_r and $\tan\delta$ for the poled BNT–BKT–BLT–x/y ceramics with $x/y = 0.05/0.10$, 0.20/0.10, 0.40/0.10, 0.15/0.05,

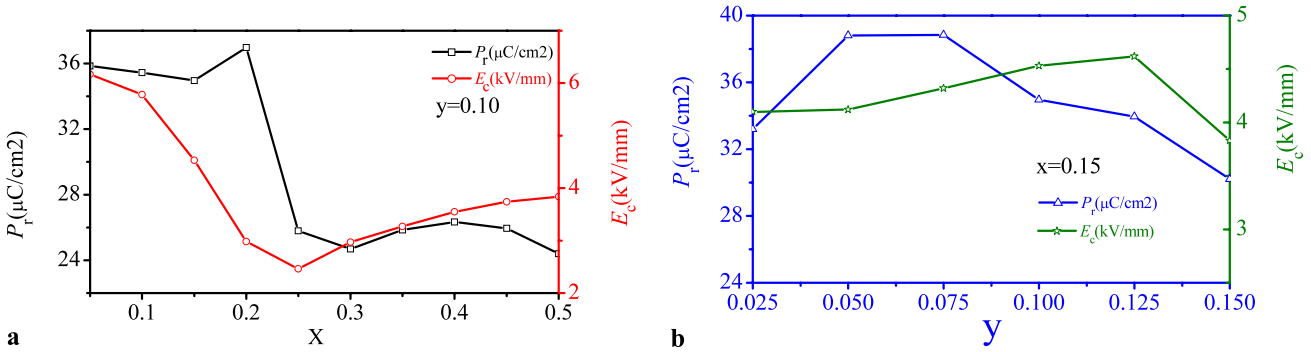

Fig. 5 Variations of P_r and E_c with x for the BNT–BKT–BLT–x/0.10 ceramics and y for the BNT–BKT–BLT–0.15/y ceramics

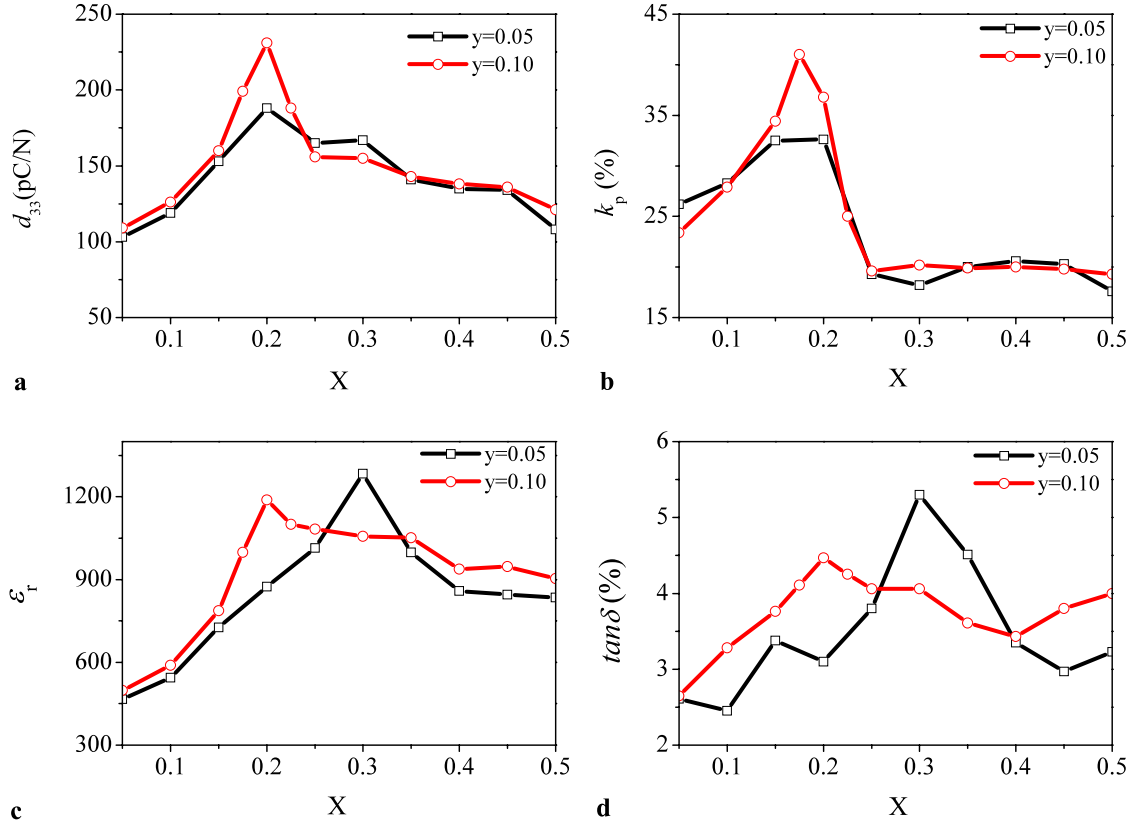

Fig. 6 Variations of d_{33}, k_p, ε_r, and $\tan\delta$ with x for the BNT–BKT–BLT–x/y ceramics ($y = 0.05$ and 0.10)

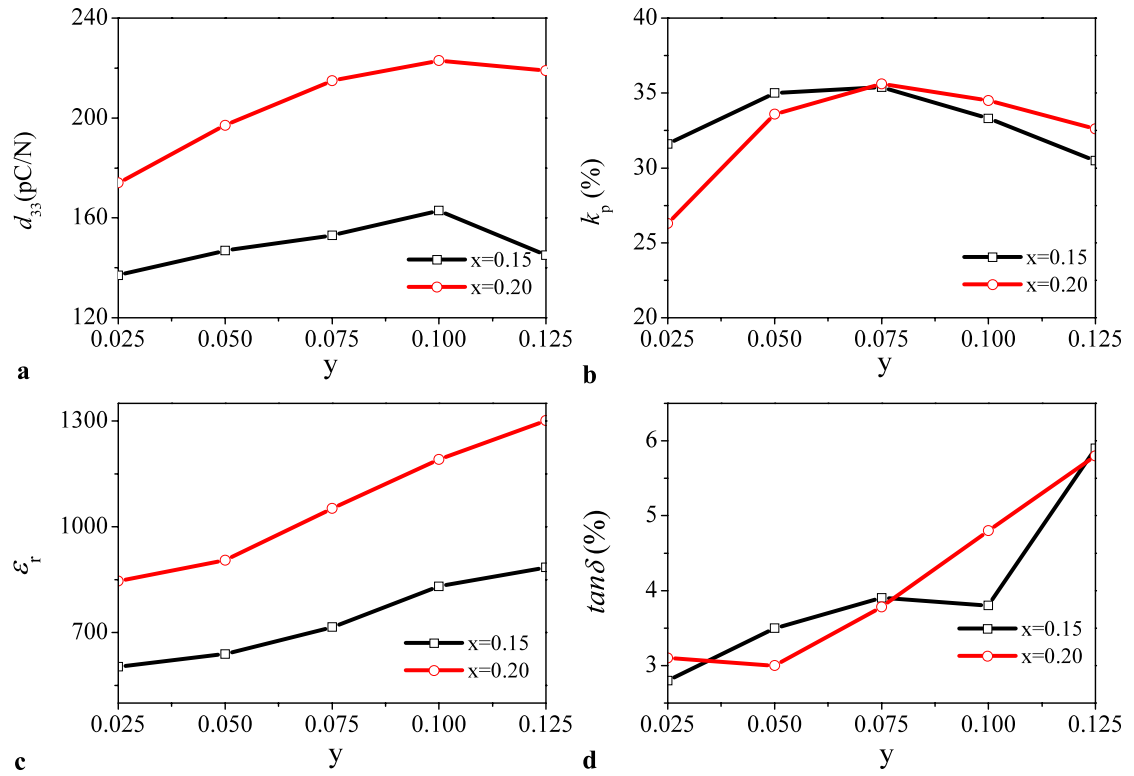

Fig. 7 Variations of d_{33}, k_p, ε_r, and $\tan\delta$ with y for the BNT–BKT–BLT–x/y ceramics ($x = 0.15$ and 0.20)

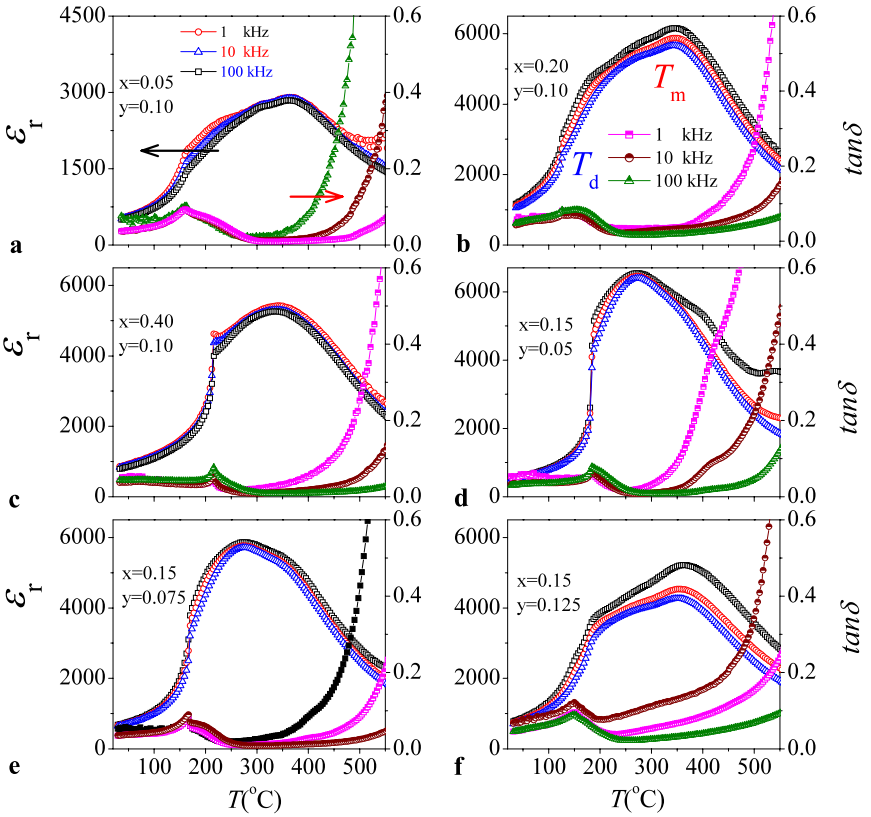

Fig. 8 Temperature dependences of ε_r and $\tan\delta$ for the BNT–BKT–BLT–x/y ceramics: (**a**) $x/y = 0.05/0.10$; (**b**) $x/y = 0.20/0.10$; (**c**) $x/y = 0.40/0.10$; (**d**) $x/y = 0.15/0.05$; (**e**) $x/y = 0.15/0.075$; and (**f**) $x/y = 0.15/0.125$

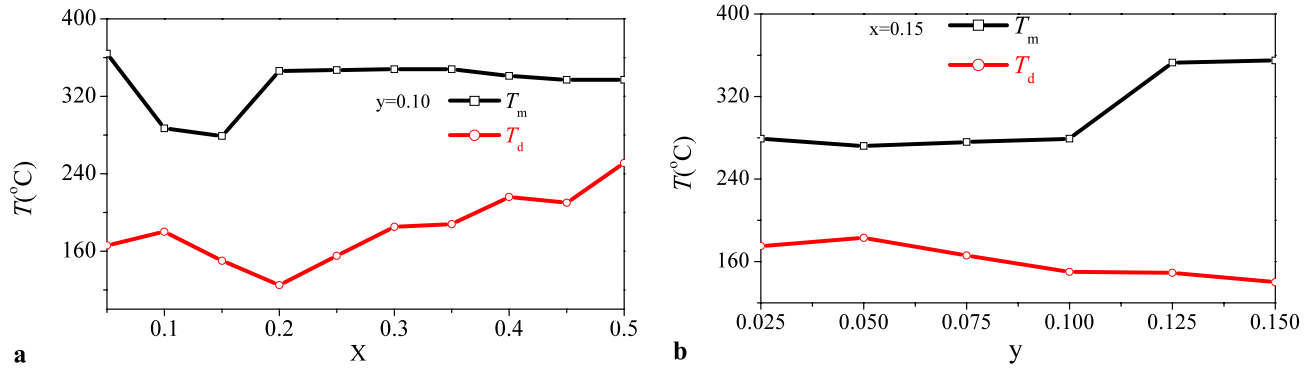

Fig. 9 Variations of T_d and T_m with x for the BNT–BKT–BLT–$x/0.10$ ceramics and y for the BNT–BKT–BLT–$0.15/y$ ceramics

0.15/0.075, and 0.15/0.125 at 1 kHz, 10 kHz, and 100 kHz. Similar to the pure BNT and other BNT-based ceramics [1–21], the ceramics exhibit two dielectric anomalies at T_d and T_m (Fig. 8). T_d is the depolarization temperature which corresponds to the transition from a ferroelectric state to so-called "anti-ferroelectric" state, while T_m is the maximum temperature at which ε_r reaches a maximum value and corresponds to a transition from an "anti-ferroelectric state" to a paraelectric state. The T_d can be derived from the temperature of $\tan\delta$'s first peak [5]. For all the ceramics, a strong frequency dependence and the broadening of the peak of ε_r at T_m suggest that the BNT–BKT–BLT–x/y ceramics are relaxor ferroelectrics. That is, the partial substitutions of K^+ and Li^+ for Na^+ in the A-site of BNT cannot change the relaxor ferroelectric characteristic of the ceramics. Relaxor phase transition has been observed in many ABO_3-type perovskites and bismuth layer-structured compounds, such as $Bi_{0.5}K_{0.5}TiO_3$ [23], $K_{0.5}La_{0.5}Bi_2Nb_2O_9$ [24] and $Pb(Sc_{0.5}Ta_{0.5})O_3$ [25], of which either the A-sites or the B-sites are occupied by at least two cations. For the BNT–BKT–BLT–x/y ceramics, Bi^{3+}, Na^+, K^+, and Li^+ are randomly distributed in the 12-fold coordination sites, so the observed relaxor behavior is reasonably attributed to the structural disordering in the arrangement of the A-site cations and the compositional fluctuation.

The variations of T_d and T_m with x and y for the BNT–BKT–BLT–x/y ceramics are shown in Fig. 9. It can be seen that for the BNT–BKT–BLT–$x/0.10$ ceramics, T_d decreases from 166 °C to 125 °C as x increases from 0.05 to 0.20, and then increases to ~258 °C with x further increasing to 0.50. It can be noted that the BNT–BKT–BLT–$x/0.10$ ceramics with $x = 0.20$ situated at the MPB possess the lowest T_d. Similar to T_d, T_m reach a minimum value of 279 °C at $x = 0.15$ (Fig. 9a). From Fig. 9b, for the BNT–BKT–BLT–$0.15/y$ ceramics, T_d decreases from 175 °C to 140 °C with y increasing from 0.025 to 0.15, while T_m keeps almost unchanged with y increasing up to $y = 0.10$ and increases quickly to 355 °C with y further increasing to 0.15. To provide additional evidence for the ferroelectric-to-"anti-ferroelectric" phase transition, the k_p of the BNT–BKT–BLT–$x/0.10$ ceramics with $x = 0.05$, 0.20, 0.30, and 0.40 have been measured at different temperatures, giving the results shown in Fig. 10. From Fig. 10, the observed k_p for all the ceramics remains almost unchanged as temperature increases, and then decreases significantly, showing clearly the ferroelectric-to-"anti-ferroelectric" phase transition. It can also be seen that the corresponding transition temperature is very close to that observed from the temperature plot of tan δ (i.e., T_d) shown in Fig. 8.

The P–E loops of the BNT–BKT–BLT–$x/0.10$ ceramics with $x = 0.05$, 0.20, 0.30, and 0.40 at different temperatures are shown in Fig. 11, while the variations of P–E

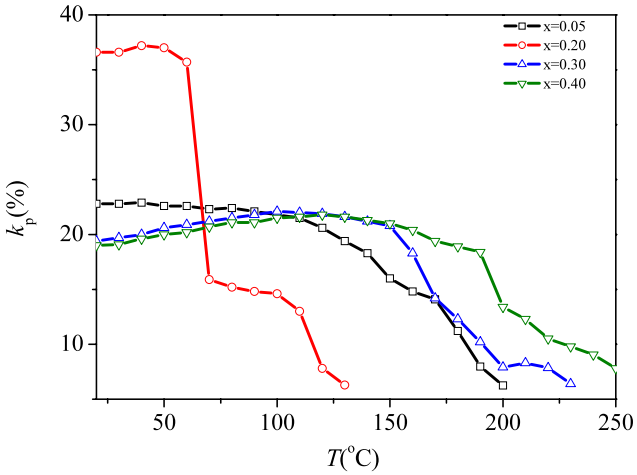

Fig. 10 Temperature dependence of k_p for the BNT–BKT–BLT–$x/0.10$ ceramics with $x = 0.05$, 0.20, 0.30, and 0.40

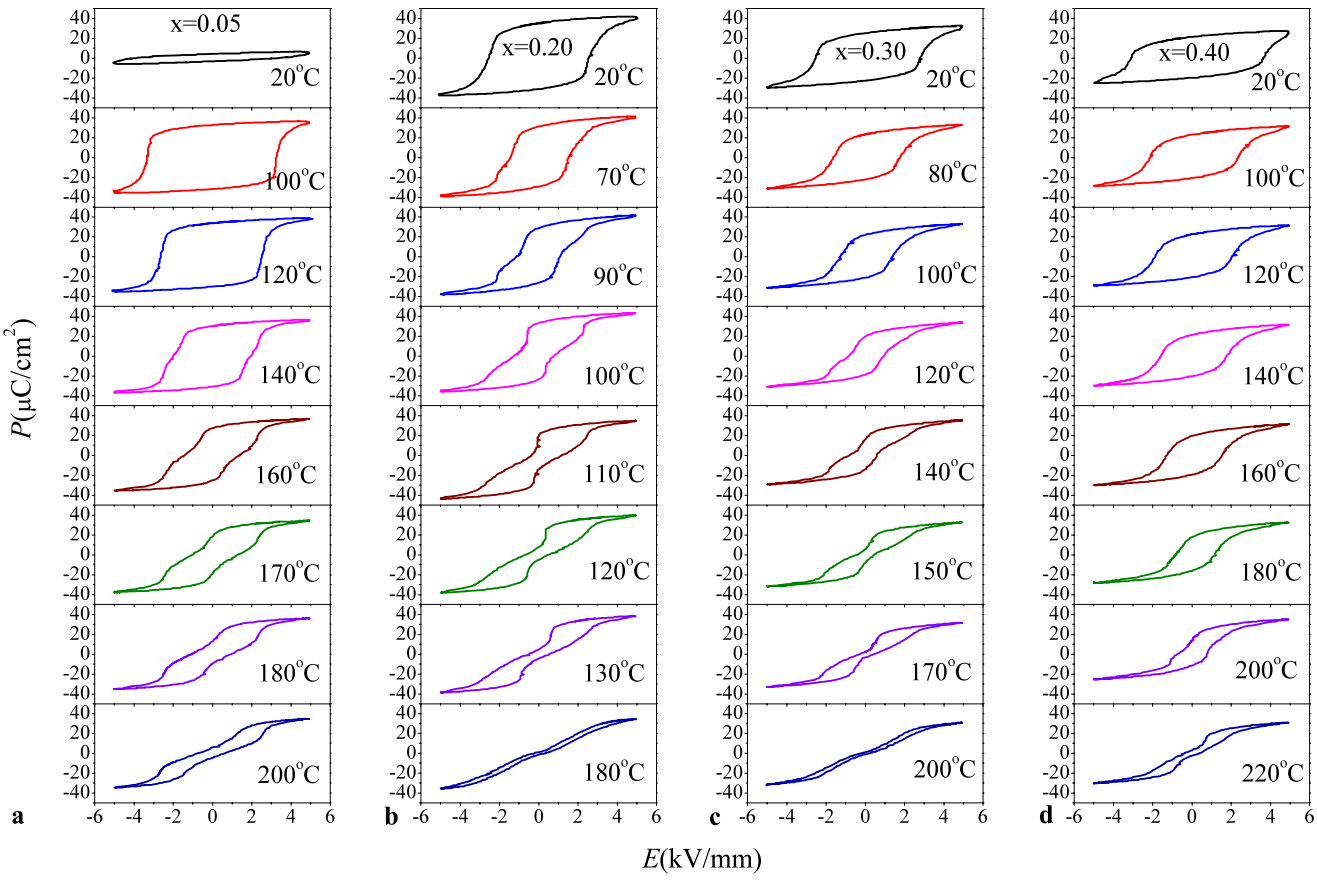

Fig. 11 Temperature dependences of P–E hysteresis loops for the BNT–BKT–BLT–$x/0.10$ ceramics: (**a**) $x = 0.05$; (**b**) $x = 0.20$; (**c**) $x = 0.30$; and (**d**) $x = 0.40$

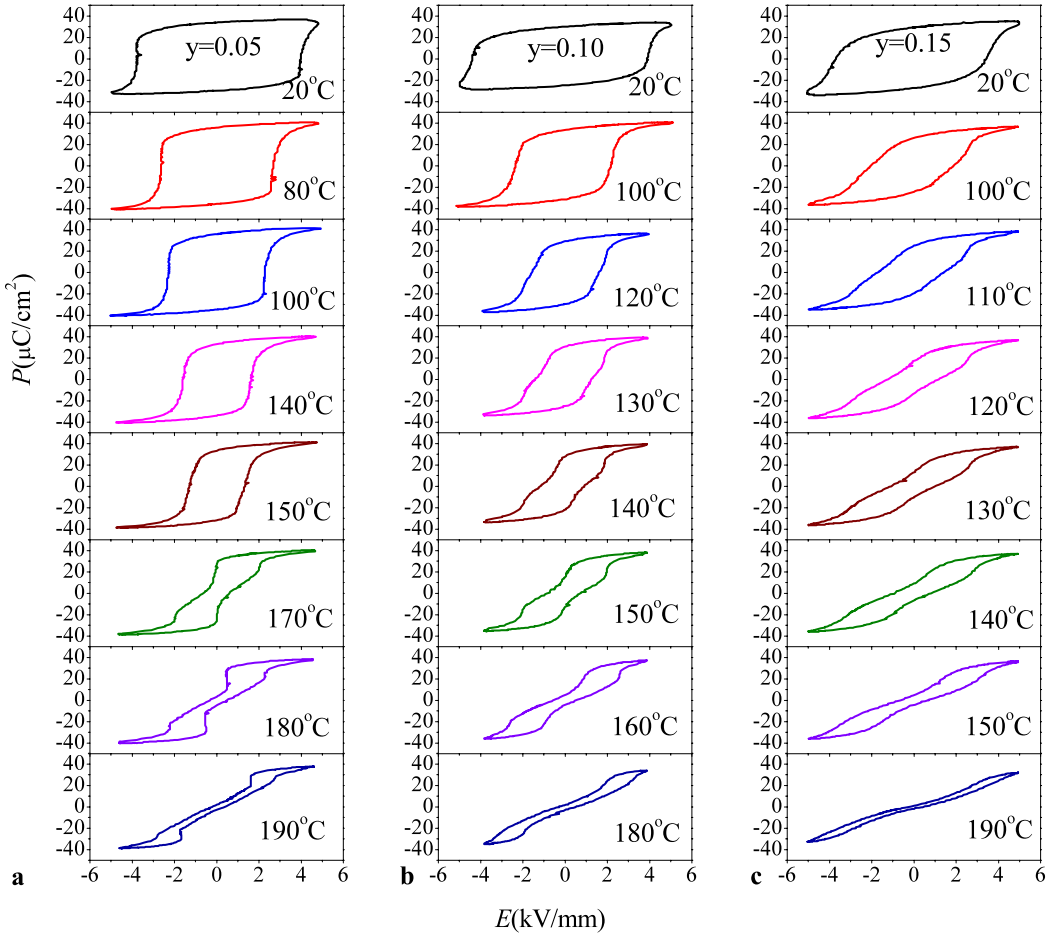

Fig. 12 P–E hysteresis loops of the BNT–BKT–BLT–0.15/y ceramics at different temperatures: (**a**) $y = 0.05$; (**b**) $y = 0.10$; and (**c**) $y = 0.15$

loops with temperature for the BNT–BKT–BLT–0.15/y ceramics with $y = 0.05$, 0.10, and 0.15 are plotted in Fig. 12. At room temperature, all the ceramics exhibit typical ferroelectric P–E loops for ferroelectrics. However, because of the high coercive field E_c (6.17 kV/mm), the P–E loop of the BNT–BKT–BLT–x/0.10 ceramics with $x = 0.05$ is not saturated under an ac field of 5 kV/mm. As temperature increases to 100 °C, the E_c of the ceramics deceases greatly (3.30 kV/mm), and thus the loop becomes relatively saturated and is well developed. The loop becomes slimmer together with the decrease in P_r and E_c with increasing temperature. At temperature above 180 °C, the loop becomes deformed and different from the typical ferroelectric characteristics and the P_r decreases significantly to 10.2 μC/cm^2. As determined from Fig. 11a, the depolarization temperature T_d of the BNT–BKT–BLT–0.05/0.10 is about 160–180 °C, which is close to the value determined from the temperature plot of tan δ (Figs. 8a and 9a). As shown in Figs. 11b–d and 12a–c, the ceramics with $x/y = 0.20/0.10$, 0.30/0.10, 0.40/0.10, 0.15/0.05, 0.15/0.10, and 0.15/0.15 exhibit similar temperature dependences of the ferroelectric properties. That is, a normal P–E loop is observed below T_d, while a deformed one is obtained at or above T_d. Similarly, the T_d values for these ceramics obtained from the temperature dependences of P–E loops are very close to those determined from the temperature plot of tan δ.

Double P–E loops have been observed in BNT-based ceramics and were suggested as the result of the transition from a ferroelectric to an anti-ferroelectric phase at T_d [2, 26]. On the other hand, deformed P–E loops have also been observed in BNT-based ceramics at high temperatures. Together with the temperature dependence of dielectric properties, it was suggested that the anomalies in P–E loop resulted from the electro–mechanical interaction between the polar and non-polar regions which coexisted in the ceramics at high temperatures [27, 28]. For the BNT–BKT–BLT–x/y ceramics, deformed P–E loops are formed at temperatures near or above T_d. At higher temperatures, although the loops are very slim, they still exhibit ferroelectric-like characteristics, not typically antiferroelectric-like (double P–E loops) for anti-ferroelectrics. So our results may imply that the tetragonal polar region and non-polar region may coexist in the BNT–BT–BLT–x/y ceramics at temperature above T_d. Further study on the phase

behavior of the ceramics at high temperature will be carried out.

4 Conclusion

A ternary K- and Li-co-modified BNT-based lead-free solid solution, $(1-x-y)Bi_{0.5}Na_{0.5}TiO_3$–$xBi_{0.5}K_{0.5}TiO_3$–$yBi_{0.5}Li_{0.5}TiO_3$, has been fabricated by an ordinary sintering technique, and its microstructure, phase transformation, electrical properties, and depolarization temperature have been studied systematically. The XRD result reveals that K^+ and Li^+ diffuse into the $Bi_{0.5}Na_{0.5}TiO_3$ lattices to form a solid solution with a pure perovskite structure, and the MPB is formed at $0.15 \leq x \leq 0.25$. The substitution of K^+ for Na^+ in the A-sites of the ceramics lowers significantly the E_c and increases slightly the P_r of the ceramics. Because of the MPB, lower E_c and larger P_r, the piezoelectricity of the ceramics is enhanced significantly. The ceramics within the MPB ($x = 0.15$–0.25 and $y = 0.50$–0.10) exhibit the optimum piezoelectricity: $d_{33} = 147$–231 pC/N and $k_P = 20.2$–41.0%. The depolarization temperature T_d has a strong dependence on the concentration level x of K^+ and the compositions situated within the MPB possess the lowest T_d. Relaxor behavior is observed in the present ceramics. It is suggested that this should result from the cation disordering in the 12-fold coordination sites. Deformed or slim P–E loops are observed at high temperatures, suggesting that polar and non-polar regions may co-exist in the ceramics at temperatures above T_d.

Acknowledgement This work was supported by the project of NSFC (50572066).

References

1. G.A. Smolenskii, V.A. Isupov, A.I. Agranovskaya, N.N. Krainik, Sov. Phys. Solid State **2**, 2651 (1961)
2. T. Takennaka, K. Maruyama, K. Sakata, Jpn. J. Appl. Phys. **30**, 2236 (1991)
3. A. Herabut, A. Safari, J. Am. Ceram. Soc. **80**(11), 2954 (1997)
4. A. Sasaki, T. Chiba, Y. Mamiya, E. Otsuki, Jpn. J. Appl. Phys. **38**(9B), 5564 (1999)
5. K. Yoshii, Y. Hiruma, H. Nagata, T. Takenaka, Jpn. J. Appl. Phys. **45**(5B), 4493 (2006)
6. S. Zhao, G. Li, A. Ding, T. Wang, Q.R. Yin, J. Phys. D: Appl. Phys. **39**, 2277 (2006)
7. Z. Yang, B. Liu, L. Wei, Y. Hou, Mater. Res. Bull. **43**, 81 (2008)
8. B.J. Chu, D.R. Chen, G.R. Li, Q.R. Yin, J. Eur. Ceram. Soc. **22**, 2115 (2002)
9. G. Fan, W. Lu, X. Wang, F. Liang, Appl. Phys. Lett. **91**, 202908 (2007)
10. Y.M. Li, W. Chen, J. Zhou, Q. Xu, H.J. Sun, R.X. Xu, Mater. Sci. Eng. B **112**, 5 (2004)
11. K. Pengpat, S. Hauphimol, S. Eitssayeam, U. Intutha, G. Rujijangul, T. Tunkasiri, J. Electroceram. **16**, 301 (2006)
12. D. Lin, D. Xiao, J. Zhu, P. Yu, J. Eur. Ceram. Soc. **26**, 3247 (2006)
13. X.X. Wang, X.G. Tang, H.L.W. Chan, Appl. Phys. Lett. **85**, 91 (2004)
14. J. Shieh, K.C. Wu, C.S. Chen, Acta Mater. **55**(9), 3081 (2007)
15. S. Zhang, T.R. Shrout, H. Nagata, Y. Hiruma, T. Takenaka, IEEE Trans. Ultrason., Ferroelect., Freq. Contr. **54**(5), 910 (2007)
16. Y. Makiuchi, R. Aoyagi, Y. Hiruma, H. Nagata, T. Takenaka, Jpn. J. Appl. Phys. **44**, 4350 (2005)
17. Y. Li, W. Chen, Q. Xu, J. Zhou, X. Gu, S. Fang, Mater. Chem. Phys. **94**, 328 (2005)
18. X.X. Wang, S.H. Choy, X.G. Tang, H.L.W. Chan, J. Appl. Phys. **97**, 104101 (2005)
19. D. Lin, K.W. Kwok, H.L.W. Chan, J. Phys. D: Appl. Phys. **40**, 5354 (2007)
20. Y.Q. Yao, T.Y. Tseng, C.C. Chou, H.H.D. Chen, J. Appl. Phys. **102**, 094102 (2007)
21. D. Lin, D. Xiao, J. Zhu, P. Yu, Appl. Phys. Lett. **88**, 062901 (2006)
22. E. Fukuchi, T. Kimura, T. Tani, Y. Saito, J. Am. Ceram. Soc. **85**(6), 1461 (2002)
23. Y. Hiruma, R. Aoyagi, H. Nagata, T. Takenaka, Jpn. J. Appl. Phys. A **44**(7), 5040 (2005)
24. C. Karthik, N. Ravishankar, K.B.R. Varma, Appl. Phys. Lett. **89**, 042905 (2006)
25. N. Setter, L.E. Cross, J. Appl. Phys. **51**, 4356 (1980)
26. J.K. Lee, J.Y. Yi, K.S. Hong, J. Sol. Stat. Chem. **177**, 2850 (2004)
27. J. Suchanicz, J. Kusz, H. Böhm, H. Duda, J.P. Mercurio, J. Eur. Ceram. Soc. **22**, 1559 (2003)
28. J. Suchanicz, J. Kusz, H. Böhm, Mater. Sci. Eng. B **97**, 154 (2003)